Development and evolution of MOEMS technology in variable optical attenuators

Chengkuo Lee
National University of Singapore
Department of Electrical & Computer Engineering
4 Engineering Drive 3
117576 Singapore
and
Institute of Microelectronics
Agency for Science, Technology and Research
(A*STAR)
11 Science Park Road
Singapore Science Park II
Singapore 117685
E-mail: elelc@nus.edu.sg

J. Andrew Yeh
National Tsing-Hua University
Institute of Nanoengineering and Microsystems
101, Section 2, Kuang Fu Road
Hsinchu, Taiwan, 30055

Abstract. Optical microelectromechanical systems (MEMS) technology or micro-optoelectromechanical systems (MOEMS) technology has proven to be an enabling technology for many components of optical networking applications. Due to their widespread applications, MEMS variable optical attenuators (VOA) have been one of the most attractive MEMS-based key devices in the optical communication market. Micromachined shutters and refractive mirrors assembled with 2D and 3D optics are the subjects of tremendous research activity. We conduct a comprehensive literature survey with respect to technologies such as fabrication processes, optical designs, actuators, and systems. Apparently, MEMS VOA technology is still evolving into a mature technology step by step. MEMS VOA technology is not only the cornerstone to support future optical communication technology, but also the best example for understanding the evolution of MOEMS technology and the commercialization of MOEMS devices. © *2008 Society of Photo-Optical Instrumentation Engineers.* [DOI: 10.1117/1.2949816]

Subject terms: microelectromechanical systems; variable optical attenuators; micro-optoelectromechanical systems; actuators.

Paper 07062SSR received Aug. 7, 2007; revised manuscript received Mar. 12, 2008; accepted for publication Mar. 27, 2008; published online Jul. 1, 2008.

1 Introduction

Since the late 1990s, the optimistic telecommunication market forecast has stimulated enormous investment in the MEMS industry, because MEMS technology has been recognized as an indispensable technology to fulfill a missing link connecting existing technologies to form an all-optical network. Telecommunication applications here become new "killer applications" of optical MEMS.[1] Many crucial MEMS-based components for telecommunication applications have been demonstrated and commercialized, such as optical switches, variable optical attenuators (VOAs), tunable filters, tunable lasers, and reconfigurable optical add/drop multiplexers. Comprehensive review articles can be referred to in Refs. 2–6, while topical reviews on optical switches[7–9] and tunable lasers[10,11] have been reported. Among these applications, VOAs and their arrays are crucial components for enabling advanced optical networks. To date, we could not find a published historical review on the technology progress or a survey report of newly updated results for VOAs. In this review article, we will conduct an extensive survey on the VOA technology evolution of the last decade. In order to have better ideas of how to apply VOAs, we present a general introduction of optical communication network architecture and features here.

The requirements for optical communication components vary with the optical networks in which they are deployed. Optical network topologies are typically categorized as three major networks: long-haul, metropolitan area, and access. Long-haul networks are the conventional long distance point-to-point transport networks that can send signals across 1000 km before the need for regeneration. Metropolitan area networks (MANs) refer to metropolitan area core ring networks that are typically hundreds of kilometers in length and typically do not use amplification. Access networks are the metropolitan area access ring networks, with stretches of a few to tens of kilometers (including the so-called "last mile"). Since the distance covered is short, amplification is not necessary. After the widespread deployment of wavelength-division-multiplexing (WDM)-based long-haul optical networks in late 1990s, WDM transmission systems have been evolving from point-to-point transmission to a next-generation, reconfigurable add/drop mesh structure. In terms of signal-to-noise ratio, power equalization is extremely important in such a system. Besides, power equalization should be performed automatically to reduce operational expenditure.

However, such technology trends drive MANs to start evolving into transparent architecture. Regarding multiple service contents in MANs, the capability of handling multiple protocols at varying speeds becomes critical to the operation efficiency of MANs. Thus, components that handle optical signals via protocol transparency and feature data rate and wavelength independence are crucial to the practical implementation of supporting this architecture. Nowadays the single-port VOA is commonly used in applications such as attenuation control on individual line cards and total signal-level control of the optical input to erbium-doped fiber amplifiers.

Typically, MEMS VOA devices offer physical features such as transparency (bit rate and protocol independent), tunability, scalability, low electrical operation power consumption, and small form factor. At nodes of MANs, the optical signals in traffic must be added into or dropped from a particular optical fiber pipeline, and can be switched

from one channel to the other, while the optical signal power of certain channels may need to be attenuated at nodes as well. Currently, the dynamic gain equalizer (DGE)[12,13] is provided in conjunction with the wavelength-division multi/demultiplexers (MUX/DEMUXs) to perform the attenuation function and the function of reconfigurable and transparent add/drop at nodes. The multichanneled VOA device can be the channel-power equalizer in WDM cross-connect nodes and in transmission networks. Thus, the integrated multichannel VOAs with MUX/DEMUXs will be an alternative to fulfill this market. In view of market requirements such as a small footprint and low power consumption, an array structure containing multiple MEMS attenuators in a single silicon chip is preferable for future DWDM applications, while single-port VOA is demanded in MAN applications.

2 MOEMS-Based Attenuation Schemes and Early Development Works

The early development of VOAs in the late 1990s was mainly performed by two groups at Lucent Technology and the group of Prof. de Rooij at the University of Neuchâtel, Switzerland. In 1994, Walker et al. developed a mechanical antireflection switch (MARS) device.[14] MARS comprises a suspended membrane with an optical window at the center of the membrane. By actuating the membrane with a displacement of $\lambda/4$, the light of a particular wavelength could be either transmitting or reflecting. The original idea was to use MARS as an optical modulator for switching functions in fiber-to-the-home applications. In 1998, Ford et al. further revised the MARS structure and applied it to the VOA application. This MARS is a silicon-nitride-suspended membrane with $\lambda/4$ optical thickness above a silicon substrate with a fixed $3\lambda/4$ spacing. Voltage applied to electrodes on top of the membrane creates an electrostatic force and pulls the membrane closer to the substrate, while the membrane tension provides a linear restoring force. When the membrane gap is reduced to $\lambda/2$, the layer becomes an antireflection coating with close to zero reflectivity. Basically, it is a quarter-wave dielectric antireflection coating suspended above a silicon substrate.[15] The membrane size varies from 100–500 μm in diameter. The mechanical resonance frequency of such a MARS device is on the order of megahertz. Thus, the response time is extremely fast, i.e., 3 μs. The dynamic range of attenuation is 25 dB. However, the insertion loss is 2 dB and wavelength-dependent loss (WDL) is relatively high for attenuation larger than 5 dB. Ford and Walker have further applied the concept of MARS to a MEMS-based DGE filter. To form the DGE filter, the optical window of the attenuator was elongated to form a suspended rectangular membrane. An array of strip-electrode pairs along the length of the optical window was arranged. By applying independently controlled voltages to all the electrode pairs, a controllable reflectivity function was developed along the length of the device. The diffraction grating-based, free-space optics system was used to spread the incoming light spectrum spatially along the length of the optical window. An input spectrum with more than a 15-dB dynamic range was flattened to less than a 0.25-dB ripple over a 42-nm wide spectrum.[12]

In contrast to the suspended dielectric antireflection membrane used in MARS, Bishop et al. lead another team at Lucent Technology in 1998 to develop a MEMS VOA using a surface-micromachined polysilicon microshutter arranged between a transmission fiber and a reception fiber aligned and located on the same axis.[16,17] In this fiber-to-fiber in-line type VOA, the shutter is connected with a movable capacitor plate via the pivoted rigid level arm, and this shutter can move upward and downward in an out-of-plane direction by adjusting the position of the capacitor plate using electrostatic force according to the applied voltage. Thereby, it can control a relative amount of attenuation by blocking parts of the light beams. This surface-micromachined in-line type MEMS VOA can achieve a dynamic range as high as 50 dB, with less than 1-dB insertion loss, while the reported shutter displacement can reach 15 μm under 3–25 V dc load. More details of these activities can be referred to in a review article by Walker.[1]

In addition to the surface-micromachined polysilicon-based approach, deep reactive ion etching (DRIE) technology is another major alternative for making MEMS VOA structures from device layers of a silicon-on-insulator (SOI) wafer. The first demonstration was done by Prof. de Rooji's group at the University of Neuchâtel, Switzerland, in 1998.[18] This SOI-based VOA device comprises a movable comb finger electrode connected with a microshutter via a suspended spring and a stationary comb-finger electrode. The attenuation range is determined in terms of the in-plane position of the Si microshutter, where this in-plane position is controlled via force balance between electrostatic force and spring force. To reduce the return loss of the input light reflected back into the input fiber, the microshutter and the fiber end faces are at an 82 deg angle with respect to the longitudinal direction of the fiber channels. This in-line-type VOA achieved insertion loss and back-reflection loss less than 1.5 dB and −37 dB, respectively, while it provided 57-dB attenuation with respect to a 32-V bias. Apparently, among these early demonstrations, the movable microshutter-based approaches exhibit promising device features, e.g., a larger dynamic range. DRIE-derived SOI MEMS VOAs have silicon trenches to accommodate optical fibers with photolithography-process-determined alignment accuracy relative to the microshutter. This feature makes the tedious assembly and alignment easier.

3 Evolution in Surface-Micromachined Mechanisms and Attenuation Schemes

Polycrystalline-silicon-based surface micromachining was initially developed for accelerometers in the early 1990s. Surface-micromachined electrostatic parallel-plate actuators, electrostatic comb actuators, electrostatic scratch drive actuators (SDA), U-shaped thermal actuators, and microstructures such as hinges and latches were demonstrated in early 1990s as well. These actuators and micromechanical elements enabled the realization of monolithically integrated free-space micro-optical benchs.[19,20] Essentially, the photon mass is not a physical concern, thus the surface-micromachined actuator just needs to manipulate the small micro-optics or micromirrors. The MARS devices of Lucent Technology relied on an electrostatic parallel-plate type of actuation,[14,15] while the first in-line-type MEMS VOA from Lucent Technology deployed a revised micro-

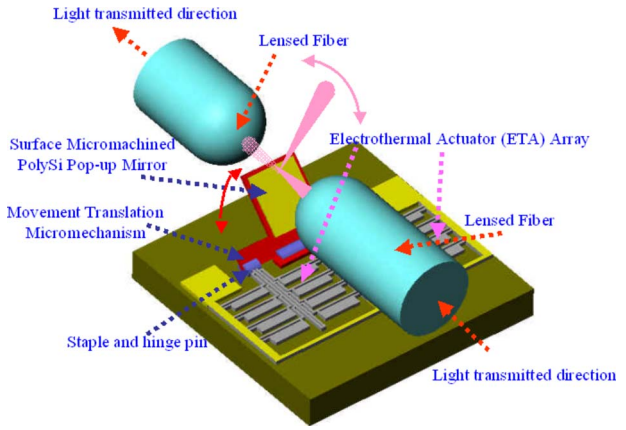

Fig. 1 Schematic drawings of a surface-micromachined MEMS VOA comprising a pop-up micromirror, and the input and output fibers. After a wet-etching release process, the lens fibers are aligned to achieve the minimum insertion loss first. The attenuated light is reflected toward the out-of-plane direction when a dc voltage is applied to the ETA array.

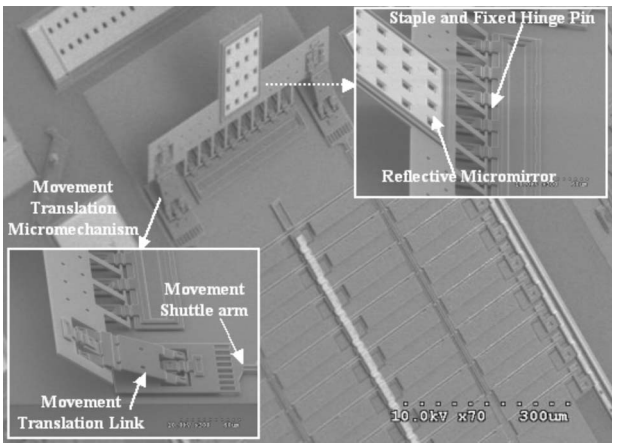

Fig. 2 SEM photograph of the MEMS VOA shows that in-plane displacement from the ETA array under dc voltage load is converted into out-of-plane rotation. The upper right inset shows a close-up view of the pop-up micromirror, staple, and fixed-hinge pin, while the bottom left inset shows a close-up view of the lifted-up MTM structure.

mechanism using an electrostatic parallel-plate type of actuation.[16,17] The demonstration of the first in-line-type MEMS VOA from Lucent Technology really showed the advantages provided by the surface micromachining technology. These merits include forming three-dimensional (3-D) complicated structures based on patterned planar layer structures, and precise control of optical alignment due to the accuracy granted by the lithography-determined planar layer structure.

In 2002, another surface-micromachined MEMS in-line-type VOA using a pop-up microshutter based on electrostatic parallel plate actuation was reported by Prof. Liu's group at Nanyang Technological University (NTU), Singapore.[21–23] Part of the pop-up microshutter uses the same design as Lucent Technology, while this microshutter is fixed on a drawbridge plate and can be moved downward to the substrate due to an applied dc bias. It demonstrates 45-dB attenuation under 8-V bias and a 1.5-dB insertion loss. Compared with Refs. 16 and 17, the driving voltage has been reduced by using this unique drawbridge structure.

In 2003, a group at Asia Pacific Microsystems, Inc. (APM) developed a new movement translation micromechanism (MTM) to convert and amplify small in-plane displacement into large out-of-plane vertical displacement or large out-of-plane rotational angle. As shown in Figs. 1 and 2, the in-plane displacement was provided by an electrically controlled electrothermal actuator (ETA) array. Based on this MTM, we applied only 3 dc V to generate 3.1-μm in-plane displacement; then a rotational angle of 26.4 deg and an equivalent out-of-plane vertical displacement of 92.7 μm for the pop-up micromirror was subsequently derived.[24,25] Using this MTM, the in-line-type VOA demonstrated a 37-dB attenuation range under a 3-V dc load, while return loss, polarization-dependent loss (PDL), and wavelength-dependent loss at an attenuation of 3 dB are measured as 45, 0.05, and 0.28 dB, respectively. This information reveals the effort of reducing driving voltage for surface-micromachined VOA devices. This study evidenced the third merit of surface micromachining to optical MEMS: a small planar displacement can be amplified into a large 3-D displacement, i.e., a large rotational angle or significant displacement of the micromirror.

However, the surface-micromachined shutter and structures are relatively fragile. During the optical fiber alignment and assembly process, these microstructures are vulnerable to damage when the optical fiber touches the microstructures unexpectedly. In view of such a concern and challenge, Lee et al. proposed a concept and design for a self-assembled VOA in 2003.[26,27] As shown in Figs. 3(a), 3(b), and 4, the self-assembly mechanism allowed a reflective shutter to be lifted up and fixed by two individually controlled stress-induced curved polysilicon beams. This self-assembled reflective shutter is then driven by a set of electrostatic SDAs so as to slide into the spacing between input and output fiber ends [Fig. 3(c) and 3(d)]. Then the attenuation is determined by the vertical position of a self-

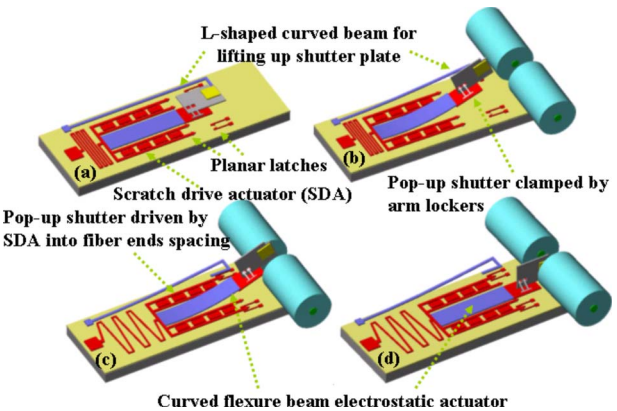

Fig. 3 Schematic drawings of self-assembled VOA with pop-up shutter and stress-induced curved beam electrostatic actuator: (a) device configuration before structure release, (b) device configuration after release and self-assembly, (c) microshutter driven by SDA and moved into the spacing between fiber ends, and (d) microshutter moved downward to perform the optical attenuation.

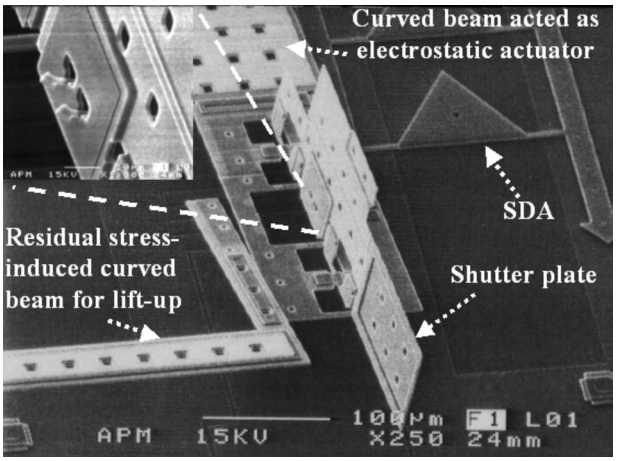

Fig. 4 The SEM photograph of MEMS VOA device with the shutter being lifted by an L-shaped stress-induced curved beam and clamped by the arrowhead locking element. The inset is the close-up view of the bottom of the shutter plate, which is clamped by the arrowhead locking elements.

assembled pop-up polysilicon reflective shutter, which is controlled by the applied dc bias. Due to the current mass-production approach for MEMS VOA, we normally place and align the input/output fibers above the MEMS chip with the v-groove trench at the beginning. The mentioned elements and/or optics are fixed at relative positions by laser welding, soldering, or UV curing. Thereafter, the assembled components are accommodated into and fixed inside product housing. As shown in Fig. 5, we propose a new manufacturing flow based on said self-assembly technology to make surface-micromachined VOA devices. First of all, we could align and fix two fibers on a silicon carrier chip with v-grooved trenches in order to get an optimized coupling efficiency, i.e., the lowest insertion loss [Fig. 5(a)]. In the mean time, the shutter plate is released and lifted, then it is fixed on a curved polysilicon beam electrostatic actuator [Fig. 5(b)]. Thereafter we could attach this self-assembled MEMS chip onto the fiber's assembled carrier chip by using flip-chip technology [Fig. 5(c)], since the shutter and peripheral-MEMS actuators and structures were designed to be allocated away from the area of fiber-to-fiber spacing. As a result, we could avoid damaging the fragile shutter and microstructures during the flip-chip assembly process. The fiber carrier chip was depicted in an opaque form in this schematic drawing to show the 3-D geometric relationship for relative elements. The v-groove-type through-wafer electrical feedthrough was also shown on the top of the assembled device chip. As shown in Fig. 5(c), we can apply the electrical load via through-wafer electrical feedthrough onto a set of SDAs located on the surrounding area of the shutter, which is hinged on a curved-beam electrostatic actuator. Since the relative positions of the fibers, actuators, and pop-up shutter were determined by photolithography accuracy, this SDA set and connected polysilicon frame will move forward, so as to drive concurrently the curved-beam electrostatic actuator and pop-up shutter moving toward the tiny spacing between the two fiber ends. Furthermore, this VOA demonstrated continuous attenuation capability, a wide attenuation range of 60 dB, and an

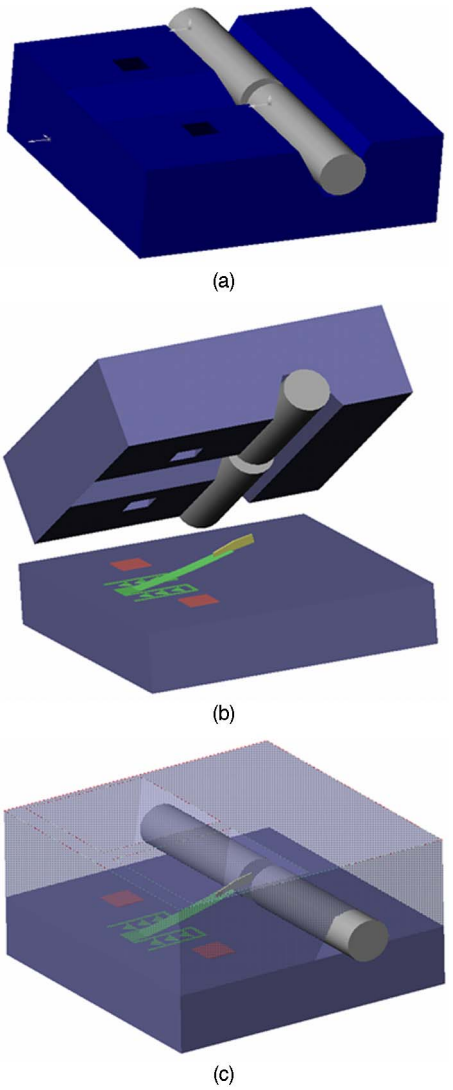

Fig. 5 Schematic drawings of the conceptualized self-assembly mechanism: (a) the fiber-aligned carrier silicon chip, (b) flip-chip assembly for bonding the fiber carrier chip and chip with a self-assembled pop-up shutter, and (c) final completed MEMS VOA, where the pop-up shutter was driven by SDA and moved into the spacing between fiber ends.

insertion loss of less than 1 dB under the 8 and 5 dc V or bright operation and dark operation, respectively. This self-assembled approach for making VOAs reveals a potential solution for getting rid of tedious optical alignment and assembly stops, while the damage of a fragile surface-micromachined polysilicon shutter could be drastically avoided.

On the other hand, Uttamchandani et al. at the University of Strathclyde have demonstrated a thermally controlled self-assembly mechanism for realizing the pop-up microshutter, while the assembled microshutter is driven by an array of SDA actuators.[28] The 45-dB attenuation could be achieved at a lateral displacement of the pop-up microshutter of about 20 μm, while the driving voltage is 60 to 290 ac V for various moving speeds of the microshutter.

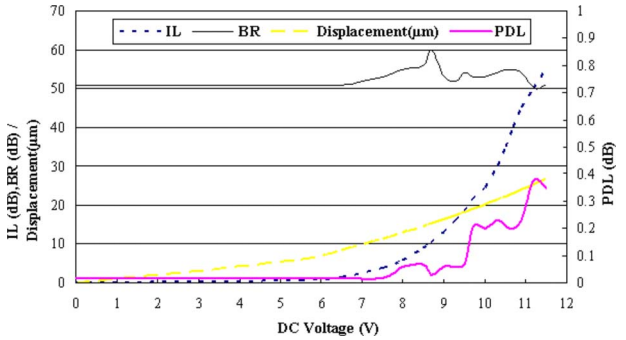

Fig. 6 Measured attenuation characteristic curves of bright operation including insertion loss (IL), return loss (denoted as BR, i.e., back-reflection loss), polarization dependant loss (PDL), and micromirror displacement versus the driving dc voltage.

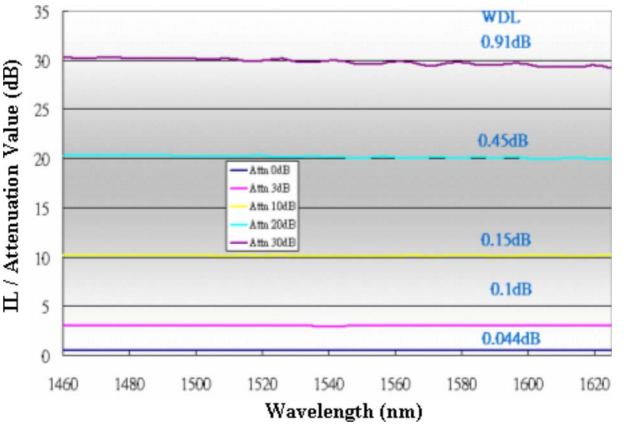

Fig. 7 Curves of wavelength-dependent loss for the single reflection-type VOA device with respect to various attenuation ranges.

4 Evolution in DRIE Mechanisms and Planar Optical-Attenuation Schemes Comprising Microshutters for Single Reflection

In contrast to the concerns discussed in the previous section about surface-micromachined VOAs, DRIE-derived VOAs from SOI substrates with fiber alignment trenches makes the testing, alignment, and assembly easier.[18] The work done at Prof. de Rooji's group really opens a window for new research activities. Since MEMS VOAs attenuate light signals in free space, the relative wavelength-dependent loss, polarization-dependent loss, and insertion loss are lower than other waveguide-based approaches, while return loss and response time can be as good as the data achieved by the other approaches (e.g., any waveguided format). However, the back-reflected light coupling into the input fiber was a concern for in-line type MEMS VOAs. In order to have smaller return loss, using fibers with 8-deg facet ends is a common solution for in-line-type VOAs. Kim et al. from Seoul National University (SNU) reported a new electrostatic comb-actuated VOA with an off-axis misalignment- based light attenuation scheme at the International Conference of Optical MEMS 2002, Lugano, Switzerland, in 2002,[29] while Lee revealed a similar design done at APM, Inc. in an invited talk at the same conference.[30] The devices made by Kim exhibited 2.5-dB insertion loss and 50-dB attenuation with respect to 14-μm displacement of the comb actuator at 5 V. Meanwhile, APM's relevant results have been published elsewhere.[31,32]

In early 2003, VOAs using off-axis misalignment, i.e., single-reflection type, typically achieved 35-dB attenuation and 50-dB attenuation under 10 to 13 V and 13 to 15 V, respectively. Kim et al. of SNU reported their progress in VOA research at the International Conference of Optical MEMS 2003, Hawaii, USA, in 2003.[33] The reported VOA achieved 35-dB attenuation at 10 V, while the maximum polarization-dependent loss was 0.24 dB within a 25-dB attenuation range. These data led performance at that time. They also reported a return loss of −38 dB, and a maximum wavelength dependent loss of 0.7 dB at 25-dB attenuation. On the other hand, Lee et al. at APM have improved the design of the electrostatic comb actuator and improved the single-reflection-type VOA. Figures 6 and 7 show the equivalent polarization-dependent loss, wavelength-dependent loss, and similar attenuation versus dc-bias characteristics. These data are about the same as results reported by Kim.[33] However, the return loss is kept smaller than −50 dB within a 50-dB dynamic range, while it is much better than the data in Ref. 33. Bashir et al. at MEMSCAP, Cairo, Egypt, also developed similar single-reflection type VOA devices.[34] Their work achieved 30-dB attenuation at 32 dc V. Within the 30-dB dynamic range, the derived polarization-dependant loss was less than 0.1 dB which was better than the data of the other groups' work.

On the other hand, for networking equipment configurations, we may need VOAs operated in a normally close scheme, i.e., dark type. Dark-type VOA means all incoming light is blocked out, i.e., 100% attenuation in the beginning. All the reported data and discussion from previous references are based on a normally open scheme, i.e., bright type. This means the initial attenuation is zero, i.e., initial insertion loss only. In order to clearly illustrate the difference in operation mechanisms for bright and dark types of VOAs with respect to in-line and single-reflection types, we explain the relationship between light paths and attenuation mechanisms first.

As shown in Fig. 8(a), which illustrains an in-line-type VOA with a slanted shutter of 8 deg, the insertion loss is maintained initially at its minimum level, and incoming light signals are fully transmitted [i.e., the upper-left drawing of Fig. 8(b)]. This shutter is approaching the light in transmission due to an applied electrical bias, then a portion of incoming light is blocked because of shutter position, as illustrated in the middle-left drawing of Fig. 8(b). The dark circle denotes the light beam, and the dotted circle represents the light-receiving area of the output port. This drawing illustrates the partially attenuated state of an in-line VOA device. Once the shutter approaches further, then all the light is fully blocked. This is the fully attenuated state as illustrated in the bottom-left drawing of Fig. 8(a). Secondly, the dark-type in-line VOA device is kept at its rest state, i.e., zero, bias state [the upper-right drawing of Fig. 8(b)]. In other words, the VOA maintains the maximum insertion loss at the beginning state, then a portion of light is allowed to transmit in response to a shift of shutter position under a certain level of electrical bias [the middle-

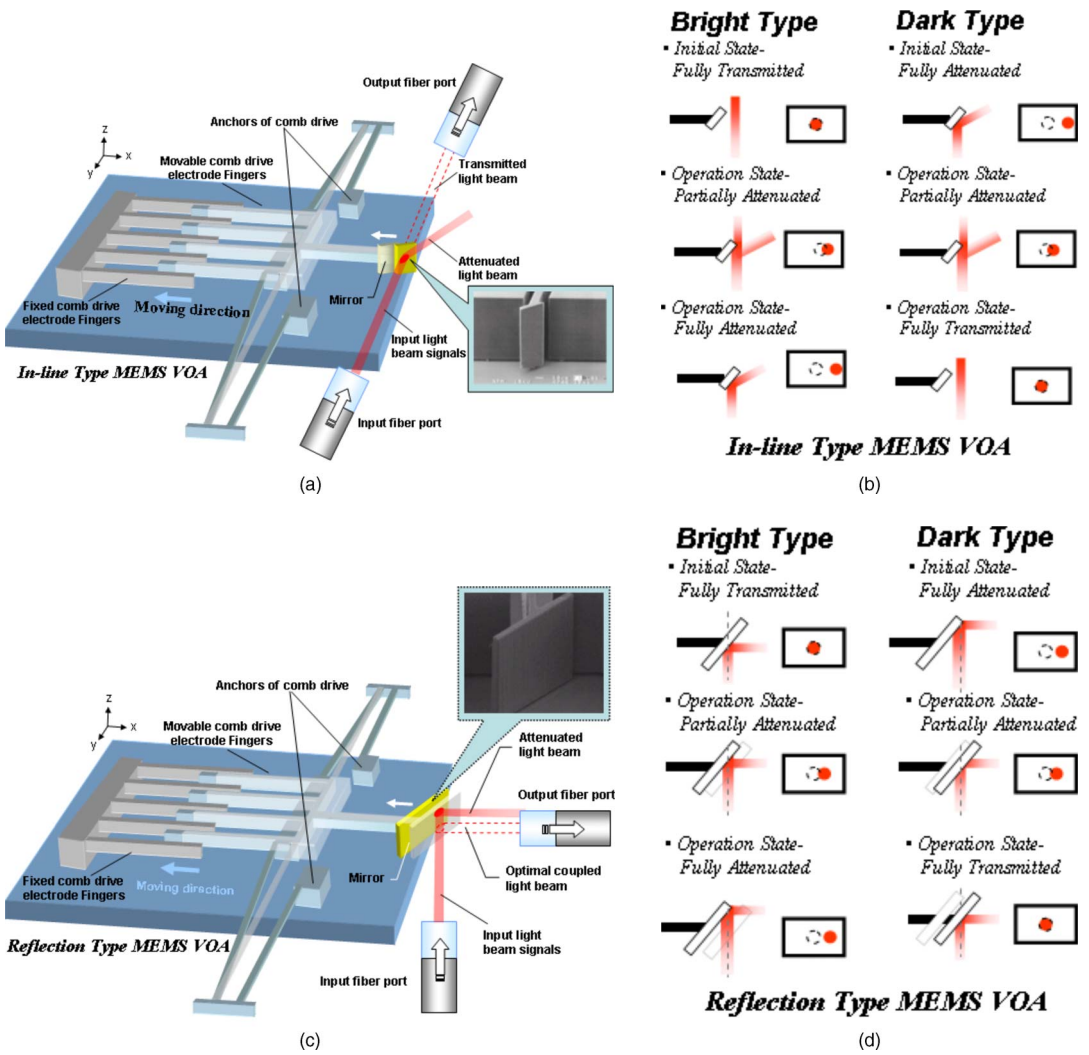

Fig. 8 (a) Schematic drawing of the in-line type MEMS VOA, where the SEM photograph of a microshutter with a mirror plane of a tilted angle is shown in the inset. (b) Schematic drawing of light path configuration based on the in-line-type attenuation scheme operated in bright and dark types. (c) Schematic drawing of the reflection-type MEMS VOA, where the SEM photograph of a reflective micromirror with a mirror plane of a 45-deg tilted angle is shown in the inset. (d) Schematic drawing of light path configuration based on the reflection-type attenuation scheme operated in bright and dark types.

right drawing of Fig. 8(b)]. When the applied electrical bias is large enough to get the shutter away from the light transmission path, all light is fully transmitted and coupled into the output port [the bottom-right drawing of Fig. 8(b)]. Secondly, Fig. 8(c) illustrates the input fiber port and output fiber port allocated in an orthogonally planar location, where the transmission light strikes a reflective mirror and is reflected toward the output port. This is the so-called reflective-type, or single-reflection, VOA. The reflected light path is changed according to different mirror positions which are determined by a comb-drive actuator according to various applied voltages; therefore, the coupled light intensity of reflected of light to the output port depends on the path of the reflected light. As shown in Fig. 8(d), the reflected light is fully coupled into the output port and fully attenuated at the beginning for bright- type operation and dark-type operation, respectively. While the partial attenuated state is considered the operation state for both bright and dark types, the actuated mirror position versus the initial rest mirror position are opposite to each other, as shown in the middle drawings of Fig. 8(d). Once the applied voltage is large enough, the reflective mirror is pulled back further, and then the reflected light path is shifted far away from the initially optimized light path. Therefore, the VOA of bright-type operation reaches its full attenuation [the bottom-left drawing of Fig. 8(d)], while the VOA of dark, type operation reaches its full transmission state [the bottom-right drawing of Fig. 8(d)].

Figure 9 shows the measured attenuation characteristics for a reflective VOA operated in a dark operation scheme. The dynamic range of 30 dB was achieved for dark-type operation under driving voltage from 5.25 to 8.25 dc V. The zero attenuation state, i.e., the full transmission state, was reached by applying 8.25 dc V for dark-type operation. The return loss, i.e., back-reflection loss (BRL), was less than −50 dB over the full span for bright type, and −48 dB for dark type, respectively. Besides, the polarization-dependent loss was derived as less than 0.15 dB within 10-dB attenu-

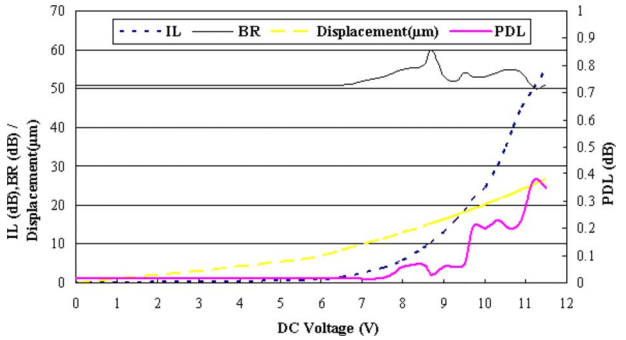

Fig. 9 Measured attenuation characteristic curves of dark operation including insertion loss (IL), return loss (denoted as BR, i.e., back-reflection loss), polarization-dependant loss (PDL), and micromirror displacement versus the driving dc voltage.

ation, less than 0.2 dB for attenuation between 10 and 20 dB, and less than 0.3 dB for attenuation between 20 and 30 dB, respectively. Briefly, the VOAs using single reflection demonstrate extremely-good polarization-dependent loss and better return loss than shutter-based VOAs. With proper design of the comb actuators, a well-optimized DRIE process, and appropriate selection of lens fibers, reflective-type VOAs are superior, except for the concern that the packaging of reflective-type VOAs with 45 deg between input and output optical fiber ports is not a common layout configuration in application markets.

5 Evolution in DRIE Mechanisms and Planar Optical-Attenuation Schemes Comprising Multiple Reflection

Regarding the layout format concern mentioned in the previous paragraph, Lee et al. of APM came up with a new retroreflective-type VOA in 2003; meanwhile a VOA of a similar concept reported by Lim et al. of LG Electronics Institute of Technology. Lim et al. created a folded mirror with 45 deg between two reflective mirrors, where this folded mirror connects with a set of comb actuators and is suspended via a silicon beam.[35] This VOA achieved 30-dB attenuation at 34 dc V. In contrast to Lim's work, APM's retroreflective-type VOAs comprised two separately controlled reflective micromirrors that are allocated in front of the input and output fibers and then assembled in a planar coaxial layout (Fig. 10). The measured characteristics exhibit an insertion loss of less than 0.9 dB, return loss of less than −50 dB, and WDL of less than 0.35-dB and 0.57-dB at 20-dB and 30-dB attenuations, respectively. The measured dynamic range of 50 dB under 7 dc V and a voltage span of 4.7 to 11 dc V was reported for bright and dark operations, respectively. The relevant results were published in 2004.[36,37] Basically, this retroreflective-attenuation mechanism results in lower operation voltage, since the intensity adjustment depends on the light path shift that is doubled after retroreflection for the same actuator driving voltage in previous reflective-type VOAs. These two micromirrors are potentially capable of being feedback controlled individually; thus, the attenuation curve could behave more linearly with dedicated control design. Besides, users in the optical communication industry are familiar with the planar coaxial layout.

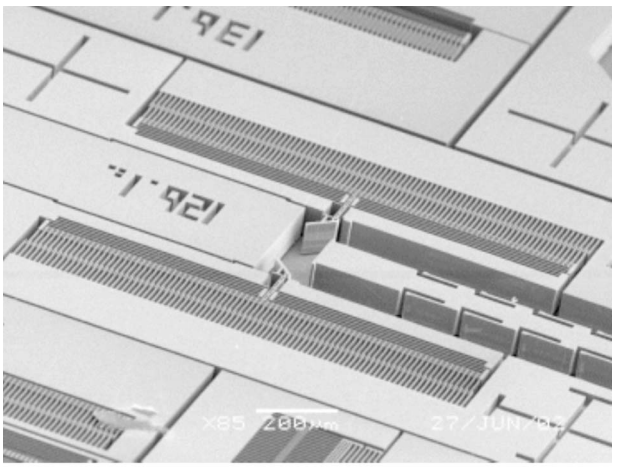

(a)

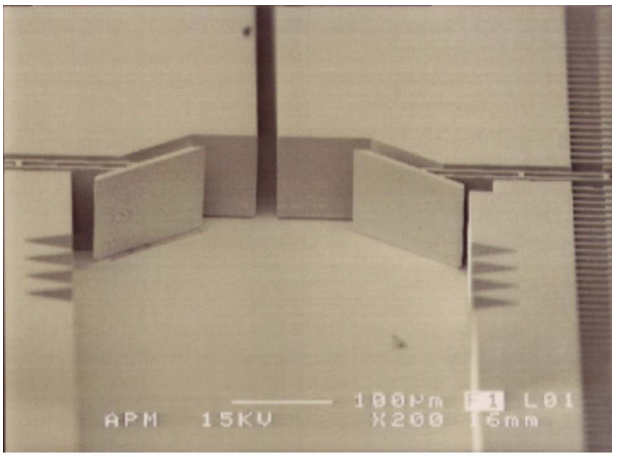

(b)

Fig. 10 SEM photographs of retroreflective-type MEMS VOA devices: (a) two reflective micromirrors and two coaxially arranged fiber trenches to form a retrorefractive-type VOA, and (b) a close-up view of micromirrors made by using DRIE of SOI substrate.

Lim et al. further explored the possibility of a driving folded mirror by using a rotary comb actuator for VOA application. This VOA comprised a folded mirror connected with a rotary comb via a suspended beam. It reported attenuation of 45 dB at a rotation angle of 2.4 deg under 21 dc V, and a response time of less than 5 ms in 2004.[38] Yeh et al. reported a reflective-type VOA.[39] This new VOA device attenuates the optical power using a planar rotational-tilted mirror driven by novel rotary comb-drive actuators. The design considerations include linear spring response, smaller moments of inertia, lower rotational spring constants, and extra optical attenuation induced by displacement in addition to rotation. A centrally symmetric structure that occupies the entire circular area was employed, and meander springs were specifically designed for desired spring responses. As shown in Fig. 11(a) and 11(b), the micromachined rotary comb-drive actuator is connected with the tilted mirror where the entire structure is suspended by four orthogonally cross-linked meander springs anchored at four corners. Four stripes of comb electrode pairs are packed in each quarter of the rotary comb-

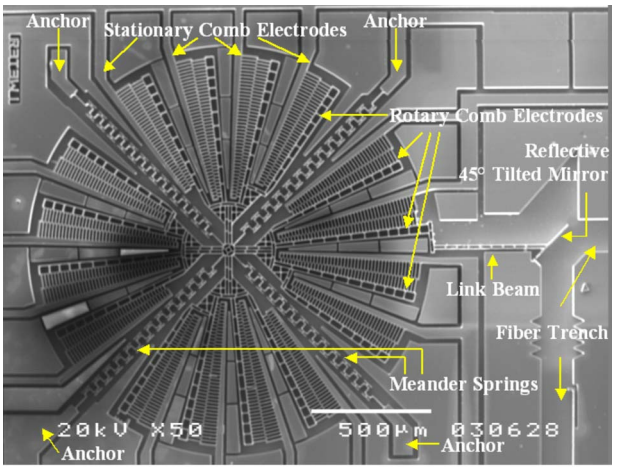

(a)

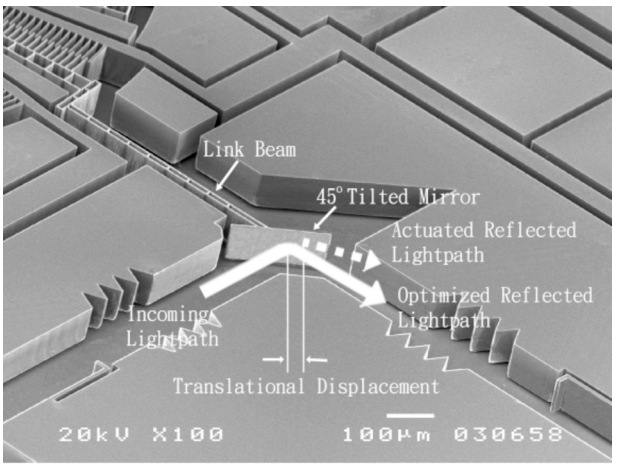

(b)

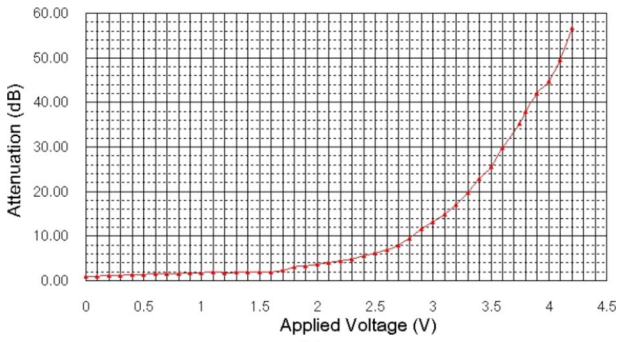

(c)

Fig. 11 (a) SEM photograph of MEMS VOA device using a rotary comb drive actuator. The VOA device has four anchors at the ends of two orthogonally located meander springs. (b) SEM photograph of a closed-up view of the rotational 45-deg tilted mirror driven by a beam linked via a rotary comb-drive actuator. (c) Measured attenuation curve versus driving voltage.

drive actuator. The meander springs are deployed to reduce the rotational spring constant K_Φ and to maintain the sufficiently large ratio of the radial spring constant K_r to the K_Φ. Hence, stable rotations at low driving voltages can be achieved along with high radial robustness in the device plane. They reported 50-dB attenuation at a rotation angle of 2.5 deg under 4.1 dc V as shown in Fig. 11(c). The response time from 0 to 40-dB attenuation and backward-switching time were measured as 3 and 0.5 ms, respectively. The measured insertion loss was 0.95 dB, and the polarization-dependent loss was 0.3 dB at 20 dB attenuation, at a wavelength of 1550 nm. The WDL was measured to be 0.19, 0.25, 0.61, and 0.87 dB for attenuation at 0, 3, 10, and 20 dB, respectively. Additionally, Kim and Kim from SNU have integrated two 45-deg reflective mirrors to form a dual-reflection-based in-line type with a minute parallel-shifted light propagation axis between input and output ports.[40] They also reported the comprehensive comparison between single-reflection VOA using lens fibers and the dual-reflection in-line-type VOA using common optical fibers.

6 Innovative Designs in Optics, Mirrors, and Actuators Based on Planar Optical-Attenuation Schemes

In 2003, a wedge-shaped silicon optical leaker, i.e., a revised shutter, was proposed as a new refractive-type VOA by Kim of Korea Aerospace Research Institute, Yun et al. of the Gwang-Ju Institute of Science and Technology, Gwangju, Korea, and Lee et al. of Samsung Electro-Mechanics Company, Suwon, Korea.[41–43] With a properly designed wedge shape, this type of shutter allows the multiple optical internal reflection to occur near the fiber core of input and output fibers. Thus, only a small portion of incoming light leaks out with a tilted propagation angle. It achieved a return loss of less than −39 dB and a wide attenuation range of 43 dB for optical fibers of 8 deg facet end, while the polarization-dependent loss was also measured to be less than 0.08, 0.43, 1.23, and 2.56 dB for the attenuation at 0.6, 10, 20, and 30 dB, respectively.

Without using a 45 deg reflective mirror, Liu's group at NTU, Singapore, proposed a novel elliptical mirror driven by an axial movable-comb actuator, where the input and output fibers were arranged and aligned in an orthogonal layout relative to said elliptical mirror.[44] In this unique design, the input and output fibers were allocated at the two focal centers of the reflective elliptical mirror. Since the ellipse can focus the light from one center to the other, the VOA enjoys low insertion loss while using the common single-mode fibers. As the mirror shifts in the direction of the axial direction of one fiber, the input beam is rapidly defocused, producing a wide attenuation range without requiring large mirror displacement. The dynamic range of 44 dB was achieved at 10.7 dc bias, while the response time was measured as 0.22 ms, respectively. The measured insertion loss was 1 dB and the polarization-dependent loss was 0.5 dB and 0.8 dB at 20-dB and 40-dB attenuations, respectively. The measured WDL was 1.3 dB at 20-dB attenuation within 1520 to 1620 nm. Without using expensive optics, e.g., lensed fibers, this new design revealed very interesting results with promising application potential. In 2007, Liu's group at NTU, Singapore, proposed an innovative design of retroreflective-type VOA using a parabolic micromirror pair.[45] They deployed a rotary mechanism to rotate this parabolic micromirror pair. The input and output fibers are arranged in parallel, while they added a rod lens in between the parabolic micromirror pair and fiber pair. The results show good linearity of attenuation

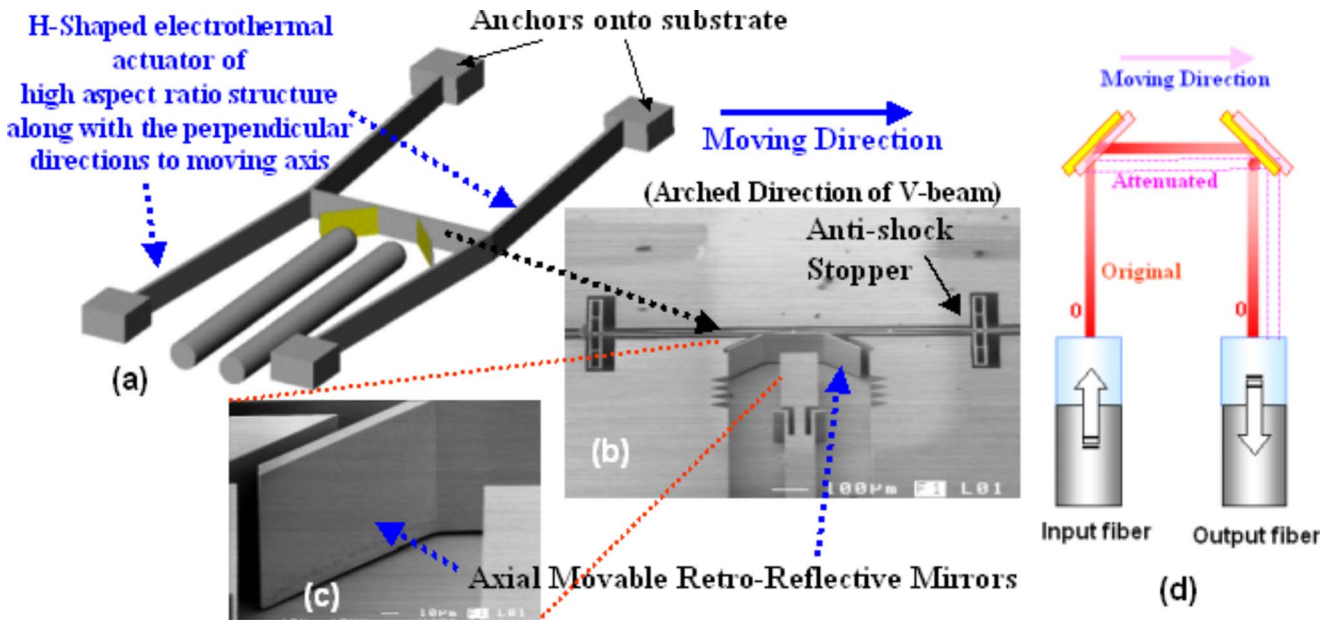

Fig. 12 VOA device comprises retroreflective mirrors driven by a linked electrothermal V-beam actuators pair, where four anchors of the V-beam actuators pair are arranged symmetrically on four corners of the device-occupied square area to form a robust VOA structure. (a) Schematic drawing, (b) SEM photograph of retroreflective mirrors and link beam, (c) SEM photograph of a closed-up view of the mirror, and (d) the retroreflective light path attenuation scheme.

versus rotation angle within the attenuation range of 60 dB, while the PDL and WDL exhibit moderate values.

As we discuss the linearity of attenuation, we should consider it in easier terms, which is the linearity of attenuation versus driving voltage curve. Regarding this issue, we have two major nonlinear factors. First of all, the moving distance of the microshutter is proportional to the square of the driving voltage of the electrostatic comb actuator. Second is that the collimated optical beam shows Gaussian distribution. Lee et al. at the Gwang-Ju Institute of Science and Technology, Gwangju, Korea, have demonstrated an in-line shutter-type VOA with linear attenuation curve using a comb actuator with a curved comb finger shape.[46] On the other hand, Liu's group at NTU, Singapore, demonstrated another way to achieve the attenuation versus driving voltage with good linearity by using two curved shutters connected with a pair of individually controlled comb actuators.[47] Liu's device shows very good linearity within 25-dB attenuation relative to 8 dc V of driving voltage. The two-shutter concept was first implemented by Chiou et al. at National Chiao Tung University, Hsinchu, Taiwan,[48] for reducing the necessary moving distance for each shutter. Thus, it could have the advantage of reduced driving voltage. Recently Glushko et al. from TeraOp, Atir Yeda, Israel, also applied this concept for gaining reduced driving voltage and compensation of nonlinearity.[49]

Until now, all the demonstrated devices have relied on electrostatic actuation mechanisms. Since no current flows between the electrodes of electrostatic actuators, it means there is no power consumption within an actuator part during operation of electrostatic actuators. However, the electrothermal actuators have been known for their large displacement and high force output. These characteristics make electrothermal actuators an alternative to serve as the actuator for VOA devices. The size and weight of MEMS elements are relatively small, and only a small amount of energy is required to operate the MEMS-based VOA. In other words, the power consumption of electrothermally driven MEMS VOA is expected to be low as well. Besides, the nature of the electrothermal actuator structure renders electrothermally driven MEMS VOAs with a smaller footprint and lighter weight than their counterpart based on electrostatic actuators. In Ref. 48, Chiou et al. deployed two pairs of U-shaped electrothermal actuators linked together to push two separated microshutters on opposite sides. Although these four U-shaped actuators have been symmetrically allocated at four corners of the device, the robustness of this VOA device is still constrained by the mechanical weakness of the flexure beam of the U-shaped actuator itself. The driving voltage was as low as 4.5 dc V at 45 dB due to the merit contributed by the two-shutter approach. As shown in Fig. 12, Lee reported an H-shaped silicon beam structure comprising two V-beam electrothermal actuators on both sides and a pair of reflective mirrors for VOA applications,[50] where this pair of mirrors are arranged at the center of a linked beam between two V-beam electrothermal actuators. When we applied the dc bias to the anchors of the V-beam, the volume expansion due to joule heating leads beams of both sides of the H-shaped beam to deform toward the arched direction, which is, denoted as the moving direction in Fig. 12. The position of the retroreflective mirrors depends on the applied bias voltage. If we applied the same bias to both V-beams, the generated displacement of both sides is the same. Optical attenuation happens when the retroreflective mirrors move from the initial location, which is optimized in terms of minimum insertion loss. The maximum dynamic range of attenuation is 50 dB under 9 dc V. The polarization-dependent loss measures as 0.15 dB at 20-dB attenuation.

Lee also demonstrated a planar attenuation micromecha-

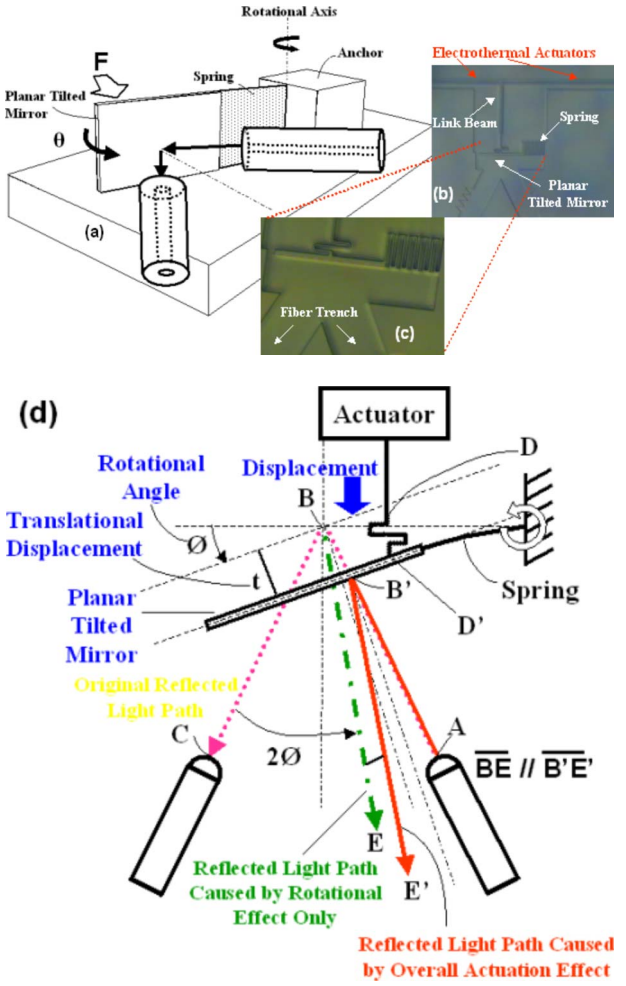

Fig. 13 VOA device comprises a planar-tilted mirror driven by a V-beam electrothermal actuator. (a) Schematic drawing, (b) CCD image of the tilted mirror, spring, link beam, and electrothermal actuator of VOA device, (c) CCD image of the tilted mirror, spring, and trenches for accommodating fibers, and (d) novel planar light-attenuation scheme is realized by using this tilted mirror with rotational and translational displacement.

nism comprising a tilted mirror driven by a V-beam electrothermal actuator via a link beam as shown in Figs. 13(a) and 13(b). This electrothermally driven tilted mirror has static displacement with a motion trace, including rotational and translational movement as shown in Fig. 13(c) and 13(d).[51] The rotational and translational misalignment of a reflected light spot toward the core of the output port fiber will lead to light attenuation. Thus the attenuation is controlled in terms of the position of the tilted mirror depending on driving dc voltage. This micromechanism granted a more efficient way of conducting the attenuation with respect to the other kinds of planar VOAs. These devices achieved 30-dB attenuation under 7.5 dc V. The PDL was less than 0.1 dB within the 30-dB attenuation region.

7 Evolution in MOEMS-Based 3D Optical-Attenuation Approaches

Combining optics and a tilted mirror (or a rotational mirror), and/or an array of mirrors to be assembled in a 3-D configuration is also a key approach of making MEMS VOA devices. Andersen et al. from Lucent Technology in 2000 reported a surface-micrmachined tilted mirror using a 3-D attenuation scheme,[52] while Riza et al. from the University of Central Florida in 1999 reported a 3-D VOA using a DMD mirror array at Texas Instruments.[53] Robinsen from Lucent Technology filed a U.S. patent in 1998 regarding this sort of idea,[54] i.e., the attenuated light is controlled by changing the tilted angle of said tilted mirror, or a portion of a mirror array in a digital manner. However, these early demonstrations only show moderate performance. In principle, we may prepare a large, single-crystalline silicon rotational mirror by using the state-of-the-art micromachining technologies.[55] When rotational mirrors are deployed for 3-D VOA in conjunction with large micro-optics, such as dual-core collimators, etc., the resulting VOA device gains excellent data of return loss, PDL, and WDL under reasonable driving voltage, i.e., small rotational angle. Toshiyoshi et al. at the University of Tokyo have demonstrated a device in which the derived performance is very good in this sense, i.e., only 4.5 dc V can achieve 0.3 deg rotational angle and 40-dB attenuation range.[56–58]

Another type of 3-D VOA uses a grating structure, i.e., the diffractive type of mechanism.[59] By modifying the original design invented by Solgaard, Lightconnect proposed a revised design using a circularly symmetric membrane structure.[60,61] This novel 3-D VOA is known as the first Telcordia-qualified MEMS VOA device. This device shows excellent response time, i.e., 40 μs, and dynamic attenuation range. We should also address the effort of digital VOA development. By using an array of digital mirrors, i.e., maintaining at either the rest position or the tilted position with a fixed deflection angle, we may individually address bias to a column of mirrors or a single mirror among said array.[62,63] The extended dynamic range of the attenuation curve is achieved up to 80 dB,[62] and the attenuation curve with good linearity can be feasibly to be derived.

8 Manufacturability and Reliability

As we discussed in the introduction, there is a demand for applying MEMS-based VOAs in multiple-channel format so as to fulfill the requirement of reconfigurable and transparent add/drop functions at nodes of an optical network. To have a monolithically integrated MEMS VOA with multiple channels means that we need very good process control in microfabrication. Using silicon DRIE to sculpt actuators and micromirrors from SOI substrates at the same time has been the most available micromachining process for VOAs. Trenches for facilitating optical fiber alignment are formed in the same DRIE step via the same photolithography mask. Such alignment trenches make the assembly and packaging work much easier. In view of such process control from the aspect of manufacturability, we have to study the nonuniformity characteristics of process-induced device performance distribution for key parameters. In 2005, Lee explored and characterized the performance of arrayed MEMS VOA devices of eight independently controlled channels, i.e., multichanneled VOA (MVOA) using in-line shutter type, reflective type,[64] and retroreflective type.[65] The number of channels is potentially scaled up to 16. As shown in Fig. 14, experimental

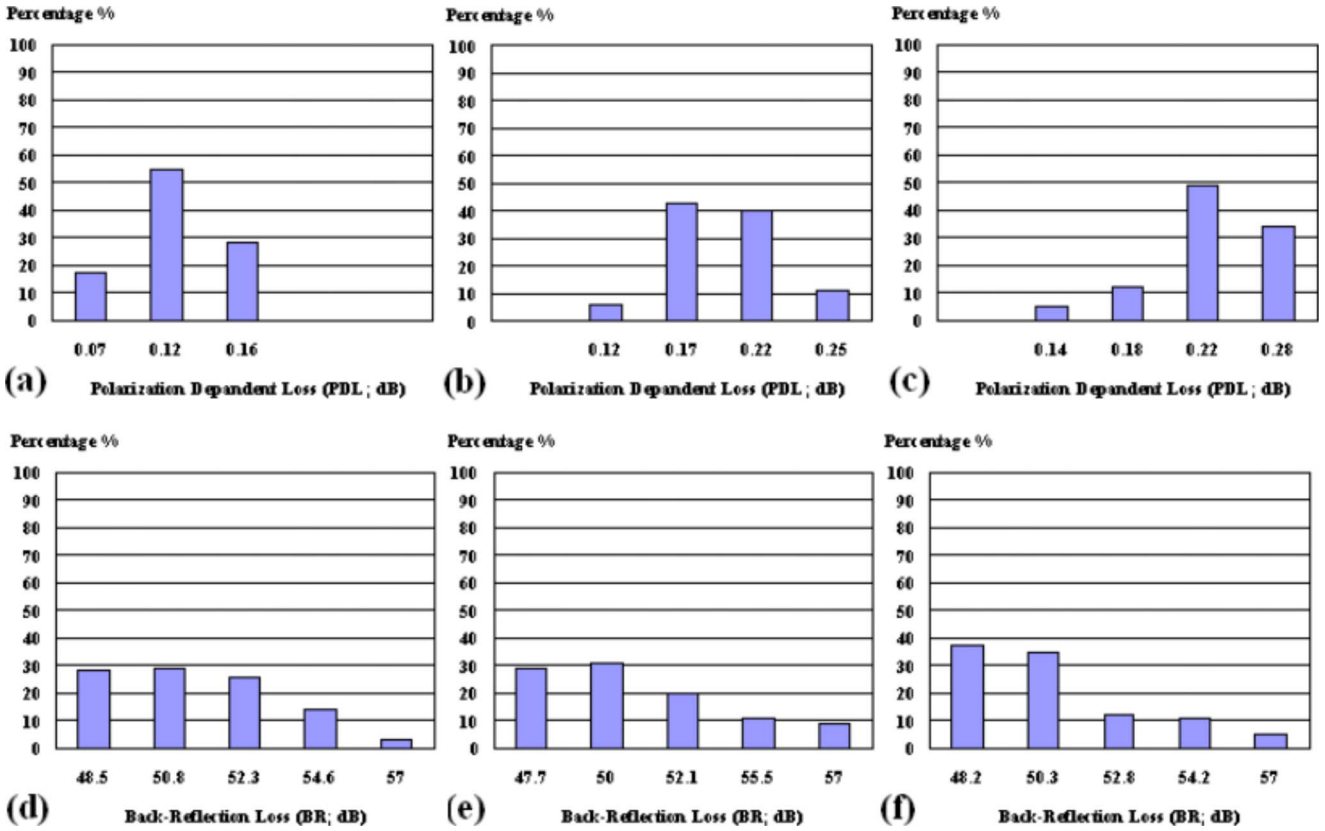

Fig. 14 Histogram of the mean value distribution of measured data from each individual channel of multichanneled VOAs using a retrorefractive attenuation scheme relative to their PDL and BRL characteristics, where (a) and (d) represent the data measured at 10-dB attenuation, (b) and (e) represent the data at 20-dB attenuation, and (c) and (f) show the data derived at 30-dB attenuation.

study of critical parameters such as insertion loss, polarization-dependent loss, return loss, and wavelength-dependent loss were characterized for several MVOA devices of monolithically integrated multichanneled configuration based on three kinds of planar light-path-attenuation schemes. Under a well-controlled process, these MVOA devices commonly provide excellent optical performance with respect to industrial common specifications. These data revealed state-of-the-art optical characteristics, while the monolithic integrated MVOA device is considered a cost-effective solution in terms of manufacturability, scalability, and an ultracompact footprint.

Moreover, the device characteristics regarding to the Telecordia GR1221 regulation are very interesting for practical applications. According to the Telecordia GR1221 regulation, the measured attenuation dynamic deviation value at 20-dB attenuation should be less than ± 0.5 dB under a vibration testing condition of 20-G periodical shocks with a frequency from 20 to 2000 Hz, along with x, y, and z axes, where four cycles of vibrations are required for each axis. In view of such a strict requirement, the H-shaped electrothermal actuation mechanism has been proposed to resolve this severe requirement, as shown in Fig. 12.[65,66] By drastically reducing the mass and enhancing the stiffness of structure, the mechanical resonant frequency of an H-shaped electrothermal VOA becomes much higher than the data of its counterpart, i.e., the electrostatic comb actuator-based designs. As listed in Table 1, the measured dynamic attenuation fluctuation is less than ± 0.03 and ± 0.15 dB at 20-dB attenuation over the full range of 20 to 2000 Hz with respect to the axes of in-plane and out-of-plane perpendicular directions to the moving axis, where the moving axis (x) is considered as the central beam with two refractive mirrors of the H-shaped structure.[66] Figure 15 shows that the measured dynamic attenuation deviation is less than ± 0.28, ± 0.30, ± 0.36, and ± 0.10 dB at vibration frequencies of 100, 500, 1000, and 2000 Hz along the mirror's moving axis, respectively. The nature of the symmetric structure of an H-shaped VOA device and the high aspect ratio of a silicon beam along with the out-of-plane

Table 1 Dynamic attenuation characteristics.

	$<\pm 0.28$ dB at 100 Hz	$<\pm 0.30$ dB at 500 Hz
Mirror moving axis	$<\pm 0.36$ dB at 1 KHz	$<\pm 0.10$ dB at 2 KHz
In-plane perpendicular axis	$<\pm 0.03$ dB	Over 20–2000 Hz
Out-of-plane perpendicular axis	$<\pm 0.15$ dB	Over 20–2000 Hz

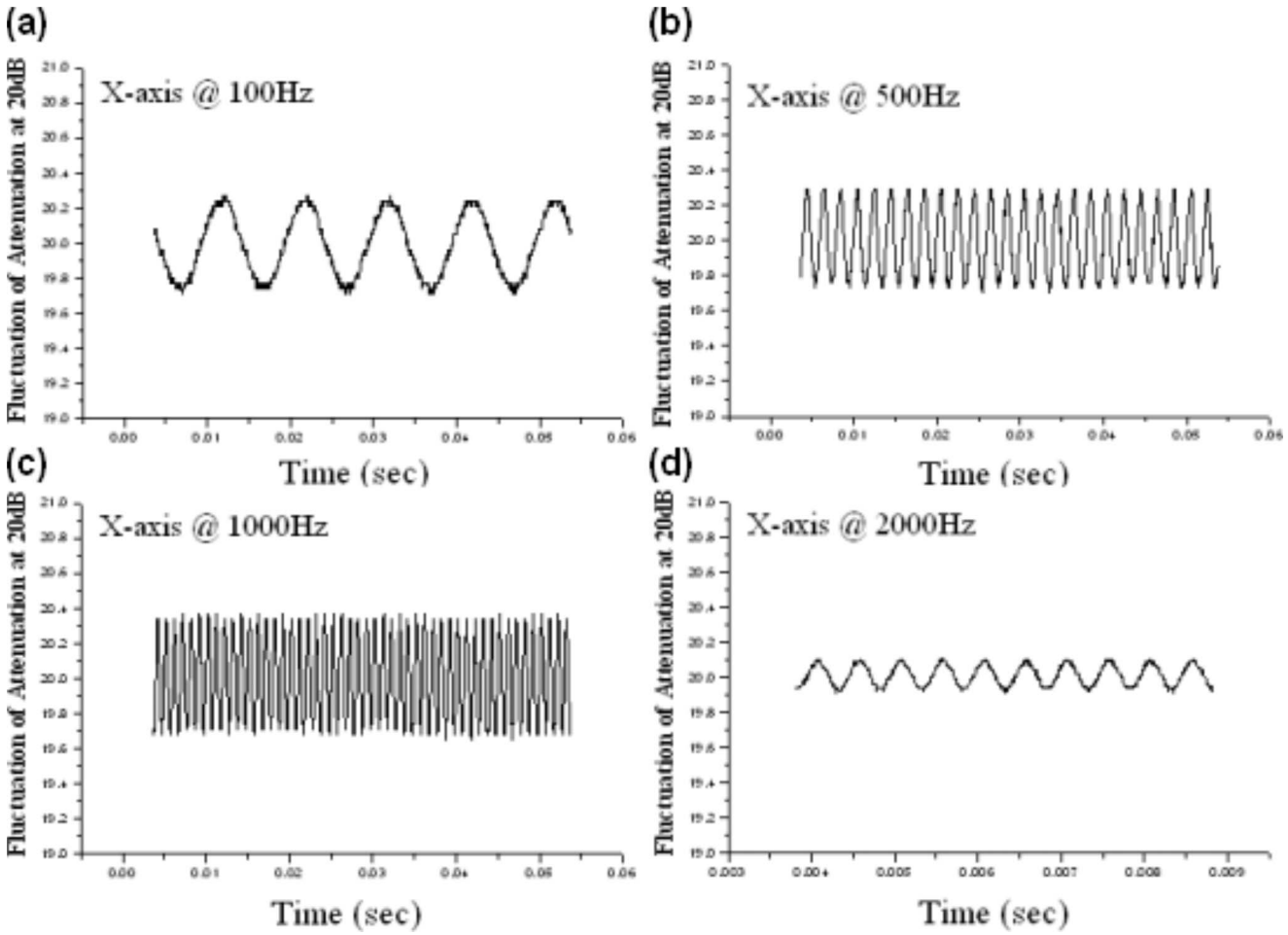

Fig. 15 Measured attenuation fluctuation value at 20-dB attenuation for a MEMS VOA using a linked pair of V-beam electrothermal actuators under mechanical vibration of 20 G along the x-axis, i.e., a mirror's moving axis, at (a) 100 Hz, (b) 500 Hz, (c) 1 KHz, and (d) 2 KHz.

perpendicular direction, i.e., the z-direction, provides excellent mechanical stability against mechanical vibrations.

The H-shaped VOA device is operated by controlling the displacement of retroreflective mirrors due to joule heating. It is natural to doubt the temperature effect on the repeatability of attenuation characteristics. Thus, Lee reported the curves of attenuation versus applied bias under different temperatures.[66] Figures 16(a)–16(c) show the temperature-dependent results of attenuation curves at 75°C, 12.5°C, and 0°C with respect to room temperature, 25°C. The revealed difference of attenuation curves is 0.5 dB, 0.6 dB and 1.3 dB for 75°C, 12.5°C and 0°C, respectively. This result is attributed to the fact that the rate of heat dissipation from an actuated and heated H-shaped beam structure becomes larger due to larger temperature differences in the case of 0°C ambient temperature. Thus, more driving voltage is required to reach the same attenuation value, where the driving electrical power is in proportion to this driving voltage. So the attenuation curve measured at 0°C ambient temperature is shifted to the right-hand side of a high-driving voltage region.

When we discuss the reliability results, we are normally looking into the measured results of packaged VOA devices. If we consider the overall loss for any occasions less than 1 dB, we may refer to the typical loss budget as an insertion loss of 0.5 dB, PDL of 0.2–0.3 dB, and package; related loss of less than 0.2 dB. The insertion loss is mainly attributed to the coupling loss between light and output port, and the reflection loss of a MEMS mirror. PDL typically gets higher at a larger attenuation range, e.g., 30-dB attenuation. Therefore, the allowable loss budget related to package and environment effects is limited to 0.2 dB. Once the device package is accomplished, proper selection of epoxy or soldering materials is crucial to maintaining accurate alignment of the optical light path among MEMS parts and optics. In other words, good matching of thermal expansion coefficients of various materials among silicon MEMS chip, optics, and housing materials is necessary. In the case of temperature-dependent VOA devices, such as H-shaped electrothermal MEMS VOAs and polymer-based VOA devices, we may deploy the heat sink structures to gain better temperature stability.[67]

A high temperature and high humidity (HTHH) aging test is one of the major test items in the Telecordia GR1209 and GR1221. It requires storage of devices at 85°C and 85% RH for 14 days (GR1209) and for 2500 h (GR1221), respectively. Hermetic sealing of housing and interface of inlet and outlet of optical fibers is definitely necessary. Without properly packaging MEMS VOA chips in hermetic housing, electrostatic comb actuator-based VOA devices

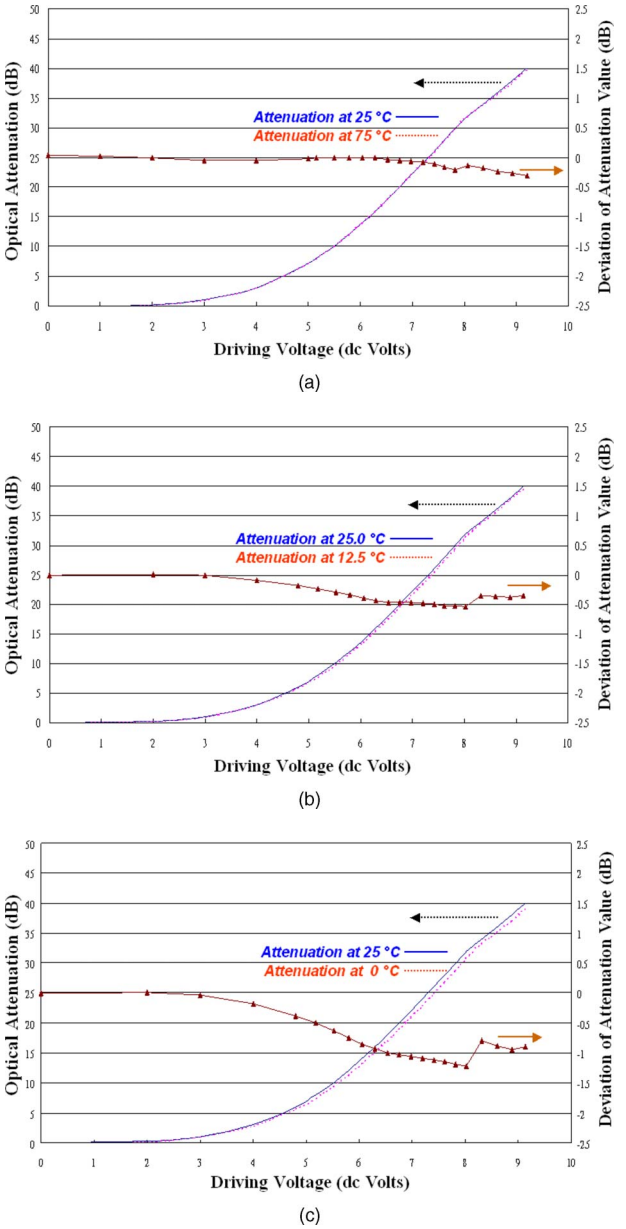

Fig. 16 Attenuation curves measured at two temperatures and curve of deviation values relative to these two attenuation curves: (a) 25 °C versus 75 °C, (b) 25 °C versus 12.5 °C, and (c) 25 °C versus 0 °C.

failed after 100 to 300 h of HTHH aging. We conclude that stiction of the comb structures is the root cause for failure after we decapsed and checked the microstructures. In contrast to electrostatic comb actuator-based VOA devices, H-shaped electrothermal MEMS VOA devices show more robust results in the HTHH aging test. However, repeatable and reliable results of VOA characteristics are normally achieved when devices are packaged in metal welding and/or soldering. Some package-related reliability data derived from waveguide-based silica VOA can be found in Ref. 67. Due to limited published MEMS VOA reliability data, we refer to the published reliability data of dry thermal aging at 85 °C for 5000 h for MEMS 2D optical switch array devices.[68]

9 Concluding Remarks

Generally speaking, approaches of planar MEMS VOA-based on DRIE-derived single crystalline microstructures show the advantages of easy assembly and repeatable manufacturability, while 3-D MEMS VOA-based solutions can easily obtain low return loss and low PDL with challenges in precise alignment and parts assembly. However, this kind of labor-intensive alignment, assembly, and packaging could be resolved by using precision automation equipment.

Various kinds of attenuation mechanisms have been demonstrated so far, while most of the actuators still use electrostatic actuators. We would also like to address some research efforts as follows: (1) Latch mechanisms allow VOAs to get rid of the requirement of on-hold voltage or power. The reported vernier-type latching mechanism for in-line shutter-type VOAs can afford as small as a 0.5-μm step resolution.[69,70] (2) Moving-fiber mechanisms can lead two aligned fibers to the misaligned positions from the optimized coupling position so as to perform the power attenuation. Thermal actuators have been reported to be good candidates as moving-fiber type of optical switches,[71–73] while electromagnetic actuation has been applied to obtain a MEMS VOA with 50-dB attenuation under only 4 V.[74] (3) Polymer waveguide or MEMS of polymer-membrane-structure-based approaches can be low-cost alternatives to enable VOAs.[75–78] Future new developments are expected as a result of this research direction. (4) Technology that enables low-cost hermetic sealing for packaging MOEMS mirrors at the wafer level for display applications is quite intriguing to MEMS VOA packaging, since we may perform the hermetical sealing of MEMS elements at the wafer level first.[79] While we can achieve MEMS wafer-level packaging, accomplishment of fiber optics assembly and interface hermetic sealing at the wafer level is the main challenge and needs to be explored.

Table 2 shows the product specifications of commercially available VOA products. Lightconnect, in Newark, California, produces a grating-based MEMS VOA device using the diffractive type of mechanism, i.e., FVOA2000.[61] This is the first MEMS VOA device that complied with Telecordia GR-1209 and GR-1221. This device shows excellent response time, i.e., 90 μs, relative to a moderate dynamic-attenuation range of 25 dB. It is worth mentioning that Lightconnect announced that their 3-D MEMS mirror-based VOA FVOA5000 passed the Telecordia GR-1209 and GR-1221 in August 2006.[61] Due to its larger mirror mass, FVOA5000 requires a 20-ms response time. Other products include 3-D MEMS reflection mirror-based products from DiCon, Richmond, California,[80] and Santec, Komaki, Aichi, Japan,[81] planar MEMS reflective mechanisms of Sercalo's VXP, and planar MEMS in-line shutter mechanisms of Sercalo's VXA.[82] The mechanisms based on reflection schemes generate better average performance than data from in-line shutter devices and 3D grating devices.

The data published to date point out the promising application potential of MEMS VOAs, since the architecture of next-generation optical communication evolves step by step into the mesh networks of the present system. New functions and requirements for MEMS VOAs may develop-us as the network evolves. As a matter of fact, we

Table 2 Specifications of commercial MEMS VOAs.

	Lightconnect (FVOA 2000)	Lightconnect (FVOA 5000)	DiCon (MEMS attenuator)	Santec (MOVA-1)	Sercalo (VXP)	Sercalo (VXA)
Mechanisms	3-D grating/ diffractive	3-D mirror/ reflection	3-D mirror/ reflection	3-D mirror/ reflection	2-D mirror/ reflection	2-D mirror/ in-line shutter
Dynamic range	25 dB	40 dB	Referred to 20 dB for measured data	30 dB	30 dB	30 dB
Insertion loss	1.0 dB max. (0.7 dB typical)	0.8 dB max. (0.4 dB typical)	0.8 dB max.	0.8 dB max.	0.9 dB max. (0.4 dB typical)	1.0 dB max. (0.6 dB typical)
Polarization-dependent loss	0.15 dB within 25 dB	0.2 dB within 40 dB (0.14 dB typical)	0.15 dB within 15 dB 0.2 dB at 15 to 20 dB	0.3 dB within 20 dB	0.15 dB within 10 dB 0.25 dB at 10 to 20 dB	0.6 dB within 10 dB 1.2 dB at 10 to 20 dB
Back-reflection loss	−45 dB	−45 dB	−50 dB max	−40 dB	−50 dB max. (−55 dB typical)	−35 dB max. (−45 dB typical)
Wavelength-dependent loss	0.3 dB max at 25 dB (0.14 dB typical)	0.1 dB max. at 10 dB (0.04 dB typical)	0.2 dB max. at 20 dB	0.5 dB max. at 10 dB 1.2 dB max. at 20 dB	0.4 dB max. at 10 dB 1.2 dB max. at 20 dB	0.4 dB max. at 10 dB 1.2 dB max. at 20 dB
Driving voltage	8 Volt	6.5 Volt	5 Volt	<20 Volts	5.25 Volt max. (5 V typical)	5.25 Volt max. (5 V typical)
Driving power	10 mW	0.5 mW	20 μW	<10 mW	30 mW max. (5 mW typical)	30 mW max. (5 mW typical)
Response time	90 μs	20 ms	2 ms max.	10 ms max.	2 ms	2 ms

refer to a market report, "Fixed and Variable Fiber-Optic Attenuators: A Worldwide Market Assessment," from KMI.[83] It reported that the worldwide optical attenuator market was expected to grow from $101 million in 2001 to nearly $600 million in 2006. VOAs were expected to occupy nearly 80% of the market's value in 2006. From the evolution of MOEMS technology in VOA and the prosperous market growth, we may build up considerable expertise and apply such knowledge to cope with commercialization issues in other MEMS devices.

Acknowledgments

This work was partially supported by grants from a joint-funded research project based on R-263-000-358-112/133 and R-263-000-475-112 of the National University of Singapore and IME's Core Project 06-420004 from the Institute of Microelectronics, A*STAR, Singapore.

References

1. J. A. Walker, "The future of MEMS in telecommunications networks," *J. Micromech. Microeng.* **10**(3), R1-R7 (2000).
2. C. R. Giles and M. Spector, "The wavelength add/drop multiplexer for lightwave communication networks," *Bell Labs Technical J.* **4**(1), 207–229 (1999).
3. A. Neukermans and R. Ramaswami, "MEMS technology for optical networking," *IEEE Commun. Mag.* **39**(1), 62–69 (2001).
4. L. Y. Lin and E. L. Goldstein, "Opportunities and challenges for MEMS in lightwave communications," *IEEE J. Sel. Top. Quantum Electron.* **8**(1), 163–172 (2002).
5. R. A. Syms and D. F. Moore, "Optical MEMS for telecoms," *Mater. Today* **5**(2), 26–35 (2002).
6. M. C. Wu, O. Solgaard, and J. E. Ford, "Optical MEMS for lightwave communication," *J. Lightwave Technol.* **24**(12), 4433–4454 (2006).
7. T.-W. Yeow, K. L. E. Law, and A. Goldenberg, "MEMS optical switches," *IEEE Commun. Mag.* **39**(11), 158–163 (2001).
8. M. Hoffmann and E. Voges, "Bulk silicon micromachining for MEMS in optical communication systems," *J. Micromech. Microeng.* **12**(4), 349–360 (2002).
9. M. Yano, F. Yamagishi, and T. Tsuda, "Optical MEMS for photonic switching-compact and stable optical crossconnect switches for simple, fast, and flexible wavelength applications in recent photonic networks," *IEEE J. Sel. Top. Quantum Electron.* **11**(2), 383–394 (2005).
10. C. J. Chang-Hasnain, "Tunable VCSEL," *IEEE J. Sel. Top. Quantum Electron.* **6**(6), 978–987 (2000).
11. A. Q. Liu and X. M. Zhang, "A review of MEMS external-cavity tunable lasers," *J. Micromech. Microeng.* **17**(1), R1-R13 (2007).
12. J. E. Ford and J. A. Walker, "Dynamic spectral power equalization using micro-opto-mechanics," *IEEE Photonics Technol. Lett.* **10**(10), 1440–1442 (1998).
13. J. E. Ford, K. W. Goossen, J. A. Walker, D. T. Neilson, D. M. Tennant, S. Y. Park, and J. W. Sulhoff, "Interference-based micromechanical spectral equalizers," *IEEE J. Sel. Top. Quantum Electron.* **10**(3), 579–587 (2004).
14. J. A. Walker, K. W. Goossen, and S. C. Arney, "Fabrication of a mechanical antireflection switch for fiber-to-the-home systems," *J. Microelectromech. Syst.* **5**(1), 45–51 (1996).
15. J. E. Ford, J. A. Walker, D. S. Greywall, and K. W. Goossen, "Micromechanical fiber-optic attenuator with 3 μs response," *J. Lightwave Technol.* **16**(9), 1663–1670 (1998).
16. B. Barber, C. R. Giles, V. Askyuk, R. Ruel, L. Stulz, and D. Bishop, "A fiber connectorized MEMS variable optical attenuator," *IEEE Photonics Technol. Lett.* **10**(9), 1262–1264 (1998).
17. C. R. Giles, V. Askyuk, B. Barber, R. Ruel, L. Stulz, and D. Bishop,

"A silicon MEMS optical switch attenuator and its use in lightwave subsystems," *IEEE J. Sel. Top. Quantum Electron.* **5**(1), 18–25 (1999).
18. C. Marxer, P. Griss, and N. F. de Rooij, "A variable optical attenuator based on silicon micromechanics," *IEEE Photonics Technol. Lett.* **11**(2), 233–235 (1999).
19. M. C. Wu, L. Y. Lin, S. S. Lee, and C. R. King, "Free-space integrated optics realized by surface-micromachining," *Int. J. High Speed Electron. Syst.* **8**(2), 283–297 (1997).
20. R. S. Muller and K. Y. Lau, "Surface-micromachined microoptical elements and systems," *Proc. IEEE* **86**(8), 1705–1720 (1998).
21. X. M. Zhang, A. Q. Liu, C. Lu, and D. Y. Tang, "MEMS variable optical attenuator using low driving voltage for DWDM systems," *Electron. Lett.* **38**(8), 382–383 (2002).
22. A. Q. Liu, X. M. Zhang, C. Lu, F. Wang, C. Lu, and Z. S. Liu, "Optical and mechanical models for a variable optical attenuator using a micromirror drawbridge," *J. Micromech. Microeng.* **13**(3), 400–411 (2003).
23. X. M. Zhang, A. Q. Liu, C. Lu, F. Wang, and Z. S. Liu, "Polysilicon micromachined fiber-optical attenuator for DWDM applications," *Sens. Actuators, A* **108**(1–3), 28–35 (2003).
24. C. Lee, Y.-S. Lin, Y.-J. Lai, M. H. Tsai, C. Chen, and C.-Y. Wu, "3-V driven pop-up micromirror for reflecting light toward out-of-plane direction for VOA applications," *IEEE Photonics Technol. Lett.* **16**(4), 1044–1046 (2004).
25. C. Lee and Y.-S. Lin, "A new micromechanism for transformation of small displacements to large rotations for a VOA," *IEEE Sens. J.* **4**(4), 503–509 (2004).
26. C. Lee, Y.-J. Lai, C.-Y. Wu, Y.-S. Lin, M. H. Tsai, R.-S. Huang, and M.-S. Lin, "Scratch drive actuator driven self-assembled variable optical attenuator," *Jpn. J. Appl. Phys., Part 1* **43**(6B), 3906–3909 (2004).
27. C. Lee, Y.-J. Lai, C.-Y. Wu, J. A. Yeh, and R.-S. Huang, "Feasibility study of self-assembly mechanism for variable optical attenuator," *J. Micromech. Microeng.* **15**(1), 55–62 (2005).
28. Lijie, J. Zawadzka, and D. Uttamchandani, "Integrated self-assembling and holding technique applied to a 3-D MEMS variable optical attenuator," *J. Microelectromech. Syst.* **13**(1), 83–90 (2004).
29. C.-H. Kim, N. Park, and Y.-K. Kim, "MEMS reflective type variable optical attenuator using off-axis misalignment," *Proc. IEEE/LEOS Int. Conf. Opt. MEMS*, pp. 55–56 (2002).
30. C. Lee, "Challenges in optical MEMS commercialization and MEMS foundry," presented at *IEEE/LEOS Int. Conf. Opt. MEMS*, Lugano, Switzerland, 20–23 August 2002, IEEE (2002).
31. C. Chen, C. Lee, Y.-J. Lai, and W.-C. Chen, "Development and application of lateral comb drive actuator," *Jpn. J. Appl. Phys., Part 1* **42**(6B), 4059–4062 (2003).
32. C. Chen, C. Lee, and Y.-J. Lai, "Novel VOA using in-plane reflective micromirror and off-axis light attenuation," *IEEE Commun. Mag.* **41**(8), S16-S20 (2003).
33. C.-H. Kim, J. Park, N. Park, and Y.-K. Kim, "MEMS fiber-optic variable optical attenuator using collimating lensed fiber," *Proc. IEEE/LEOS Int. Conf. Opt. MEMS*, pp. 145–146 (2003).
34. A. Bashir, P. Katila, N. Ogier, B. Saadany, and D. A. Khalil, "A MEMS-based VOA with very low PDL," *IEEE Photonics Technol. Lett.* **16**(4), 1047–1049 (2004).
35. T.-S. Lim, C.-H. Ji, C.-H. Oh, Y. Yee, and J. U. Bu, "Electrostatic MEMS variable optical attenuator with folded micromirror," *Proc. IEEE/LEOS Int. Conf. Opt. MEMS*, pp. 143–144 (2003).
36. C. Lee, M. H. Tsai, C.-Y. Wu, S.-Y. Hung, C. Chen, Y.-J. Lai, M.-S. Lin, and J. Andrew Yeh, "Characterization of MOEMS VOA based on various planar light attenuation configurations," *Proc. IEEE/LEOS Int. Conf. Opt. MEMS*, pp. 98–99 (2004).
37. C. Chen, C. Lee, and J. Andrew Yeh, "Retro-reflection type MOEMS VOA," *IEEE Photonics Technol. Lett.* **16**(10), 2290–2292 (2004).
38. T.-S. Lim, C.-H. Ji, C.-H. Oh, H. Kwon, Y. Yee, and J. U. Bu, "Electrostatic MEMS variable optical attenuator with rotating folded micromirror," *IEEE J. Sel. Top. Quantum Electron.* **10**(3), 558–562 (2004).
39. J. A. Yeh, S.-S. Jiang, and C. Lee, "MOEMS VOA using rotary comb drive actuators," *IEEE Photonics Technol. Lett.* **18**(10), 1170–1172 (2006).
40. C.-H. Kim and Y.-K. Kim, "MEMS variable optical attenuator using translation motion of 45-deg tilted vertical mirror," *J. Micromech. Microeng.* **15**(8), 1466–1475 (2005).
41. J. H. Lee, Y. Y. Kim, S. S. Yun, H. Kwon, Y. S. Hong, J. H. Lee, and S. C. Jung, "Design and characteristics of a micromachined variable optical attenuator with a silicon optical wedge," *Opt. Commun.* **221**(4–6), 323–330 (2003).
42. Y. Y. Kim, S. S. Yun, C. S. Park, J.-H. Lee, Y. G. Lee, H. K. Lee, S. K. Yoon, and J. S. Kang, "Refractive variable optical attenuator fabricated by silicon deep reactive ion etching," *IEEE Photonics Technol. Lett.* **16**(2), 485–487 (2004).
43. J. H. Lee, S. S. Yun, Y. Y. Kim, and K.-W. Jo, "Optical characteristics of a refractive optical attenuator with respect to the wedge angles of a silicon optical leaker," *Appl. Opt.* **43**(4), 877–882 (2004).
44. H. Cai, X. M. Zhang, C. Lu, A. Q. Liu, and E. H. Khoo, "Linear MEMS variable optical attenuator using reflective elliptical mirror," *IEEE Photonics Technol. Lett.* **17**(2), 402–404 (2005).
45. X. M. Zhang, A. Q. Liu, H. Cai, A. B. Yu, and C. Lu, "Retro-axial VOA using parabolic mirror pair," *IEEE Photonics Technol. Lett.* **19**(9), 692–694 (2007).
46. M. G. Kim and J.-H. Lee, "A discrete positioning microactuator: linearity modeling and VOA application," *J. Microelectromech. Syst.* **16**(1), 16–23 (2007).
47. Q. W. Zhao, X. M. Zhang, A. Q. Liu, H. Cai, J. Zhang, and C. Lu, "Theoretical and experimental studies of MEMS dual-shutter VOA for linear attenuation relationship and ultra-fine tuning," *J. Lightwave Technol.*. **26**(5), 569–579 (2008).
48. J. C. Chiou and W. T. Lin, "Variable optical attenuator using a thermal actuator array with dual shutters," *Opt. Commun.* **237**(4–6), 341–350 (2004).
49. B. Glushko, S. Krylov, M. Medina, and D. Kin, "Insertion type MEMS VOA with two transparent shutters," *Proc. Asia-Pacific Conf. Transducers Micro-Nano Technol. (APCOT)*, Paper No. 95-OMN-A0594 (2006).
50. C. Lee, "MOEMS variable optical attenuator with robust design for improved dynamic characteristics," *IEEE Photonics Technol. Lett.* **18**(6), 773–775 (2006).
51. C. Lee, "Variable optical attenuator using planar light attenuation scheme based on rotational and translational misalignment," *Microsyst. Technol.* **13**(1), 41–48 (2007).
52. B. M. Andersen, S. Fairchild, N. Thorsten, and V. Aksyuk, "MEMS variable optical amplifiers," *Proc. Opt. Fiber Commun. Conf.* **2**, 260–262 (2000).
53. N. A. Riza and S. Sumriddetchkajorn, "Digitally controlled fault-tolerant multiwavelength programmable fiber-optic attenuator using a two-dimensional digital micromirror device," *Opt. Lett.* **24**(5), 282–284 (1999).
54. K. C. Robinson, "Variable optical attenuator," U.S. Patent No. 6137941 (2000).
55. H. Schenk, A. Wolter, U. Dauderstaedt, A. Gehner, and H. Lakner, "Microoptoelectromechanical systems technology and its impact on photonic applications," *J. Microlithogr., Microfabr., Microsyst.* **4**(4), 041501 (2005).
56. K. Isamoto, K. Kato, A. Morosawa, C. Chong, H. Fujita, and H. Toshiyoshi, "Micromechanical VOA design for high shock-tolerance and low temperature-dependence," *Proc. IEEE/LEOS Int. Conf. Opt. MEMS*, pp. 113–114 (2003).
57. K. Isamoto, K. Kato, A. Morosawa, C. Chong, H. Fujita, and H. Toshiyoshi, "A 5-Voperated MEMS variable optical attenuator by SOI bulk micromachining," *IEEE J. Sel. Top. Quantum Electron.* **10**(3), 570–578 (2004).
58. K. Isamoto, A. Morosawa, M. Tei, H. Fujita, and H. Toshiyoshi, "MEMS variable optical attenuator using asymmetrically driven parallel plate tilt mirror," *IEEJ Trans. Sars. Micromech.* **124**(6), 213–218 (2004).
59. O. Solgaard, F. S. A. Sandejas, and D. M. Bloom, "Deformable grating optical modulator," *Opt. Lett.* **17**(9), 688–690 (1992).
60. A. Godil, "Diffractive MEMS technology offers a new platform for optical networks," *Laser Focus World* **38**(5), 181–185 (2002).
61. http://www.lightconnect.com/.
62. N. A. Riza and F. N. Ghauri, "Hybrid analog-digital MEMS fiber-optic variable attenuator," *IEEE Photonics Technol. Lett.* **17**(1), 124–126 (2005).
63. W. Sun, W. Noell, M. Zickar, M. J. Mughal, F. Perez, N. A. Riza, and N. F. de Rooij, "Design, simulation, fabrication, and characterization of a digital variable optical attenuator," *J. Microelectromech. Syst.* **15**(5), 1190–1200 (2006).
64. C. Lee, "Monolithic-integrated 8CH MEMS variable optical attenuators," *Sens. Actuators, A* **123–124**, 596–601 (2005).
65. C. Lee, "Arrayed variable optical attenuator using retro-reflective MEMS mirrors," *IEEE Photonics Technol. Lett.* **17**(12), 2640–2642 (2005).
66. C. Lee, "A MEMS VOA using electrothermal actuators," *J. Lightwave Technol.* **25**(2), 490–498 (2007).
67. I. Ogawa, Y. Doi, Y. Hashizume, S. Kamei, Y. Tamura, M. Ishii, T. Kominato, H. Yamazaki, and A. Kaneko, "Packaging technology for ultra-small variable optical attenuator multiplexer (V-AWG) with multichip plc integration structure using chip-scale-package PD array," *IEEE J. Sel. Top. Quantum Electron.* **12**(5), 1045–1053 (2006).
68. P. De Dobbelaere, K. Falta, and S. Gloeckner, "Advances in integrated 2D MEMS-based solutions for optical network applications," *IEEE Commun. Mag.* **41**(5), S16–S23 (2003).
69. R. R. A. Syms, H. Zou, J. Stagg, and D. F. Moore, "Multistate latching MEMS variable optical attenuator," *IEEE Photonics Technol. Lett.* **16**(1), 191–193 (2004).
70. R. R. A. Syms, H. Zou, and P. Boyle, "Mechanical stability of a latching MEMS variable optical attenuator," *J. Microelectromech. Syst.* **14**(3), 529–538 (2005).

71. A. Unamuno and D. Uttamchandani, "MEMS variable optical attenuator with vernier latching mechanism," *IEEE Photonics Technol. Lett.* **18**(1), 88–90 (2006).
72. M. Hoffmann, P. Kopka, T. Groβ, and E. Voges, "Optical fibre switches based on full wafer silicon micromachining," *J. Micromech. Microeng.* **9** (2), 151–155 (1999).
73. K. R. Cochran, L. Fan, and D. L. DeVoe, "High-power optical micro switch fabricated by deep reactive ion etching (DRIE)," *Proc. SPIE* **4983**, 75–86 (2003).
74. X. Dai, X. Zhao, G. Ding, and B. Cai, "Micromachined electromagnetic variable optical attenuator for optical power equalization," *J. Microlithogr., Microfabr., Microsyst.* **4**(4), 041304 (2005).
75. S.-S. Lee, J.-U. Bu, S.-Y. Lee, K.-C. Song, C.-G. Park, and T.-S. Kim, "Low-power consumption polymeric attenuator using a micromachined membrane-type waveguide," *IEEE Photonics Technol. Lett.* **12**(4), 407–409 (2000).
76. M.-C. Oh, S.-H. Cho, Y.-O. Noh, H.-J. Lee, J.-J. Joo, and M.-H. Lee, "Variable optical attenuator based on large-core single-mode polymer waveguide," *IEEE Photonics Technol. Lett.* **17**(9), 1890–1892 (2005).
77. S. K. Kim, Y.-C. Hung, K. Geary, W. Yuan, H. R. Fetterman, D. Jin, R. Dinu, and W. H. Steier, "Metal-defined polymeric variable optical attenuator," *IEEE Photonics Technol. Lett.* **18**(9), 1055–1057 (2006).
78. G.-D. J. Su, Y.-W. Yeh, C.-W. E. Chiu, C.-H. Li, and T.-Y. Chen, "Fabrication and measurement of low-stress polyimide membrane for high resolution variable optical attenuator," *IEEE J. Sel. Top. Quantum Electron.* **13**(2), 312–315 (2007).
79. H. van Heeren, A. EI-Fatatry, L. Paschalidou, and P. Salomon, "Industrial packaging and assembly infrarstructure for MOEMS," *J. Microlithogr., Microfabr., Microsyst.* **4**(4), 041701 (2005).
80. http://www.diconfiberoptics.com/.
81. http://www.santec.com/.
82. http://www.sercalo.com/.
83. http:/www.kmicorp.com/.

Biographies and photographs of the authors not available.